Title

Transgressive deposits along the actively deforming Eel River Margin, Northern California

Journal

Marine Geology, 303

ISSN

0025-3227

Authors

Hogarth, Leah J
Driscoll, Neal W
Babcock, Jeffrey M
et al.

Publication Date

2012-03-01

DOI

10.1016/j.margeo.2012.02.005

Peer reviewed

Marine Geology 303–306 (2012) 99–114

Contents lists available at SciVerse ScienceDirect

Marine Geology

journal homepage: www.elsevier.com/locate/margeo

Transgressive deposits along the actively deforming Eel River Margin, Northern California

Leah J. Hogarth [a,*], Neal W. Driscoll [a], Jeffrey M. Babcock [a], Daniel L. Orange [b]

[a] *Scripps Institution of Oceanography, UCSD, 9500 Gilman Drive, La Jolla, CA 92093-0244, USA*
[b] *Niko Resources Ltd, Plaza City View 5th Floor, Jalan Kemang Timur No. 22, Jakarta 12510, Indonesia, Indonesia*

ARTICLE INFO

Article history:
Received 2 July 2010
Received in revised form 2 February 2012
Accepted 11 February 2012
Available online 18 February 2012

Communicated by D.J.W. Piper

Keywords:
Mendocino Triple Junction
Eel River Basin
Little Salmon Fault
transgressive deposits
active deformation

ABSTRACT

New high-resolution CHIRP seismic data acquired along the Eel River margin, northern California, reveal that stratal architecture and sediment thickness of the Holocene transgressive deposits are, in large part, controlled by tectonic deformation and sediment supply. A thick (>20 m) transgressive deposit is observed across the Eel margin, a forearc basin that is undergoing active folding perpendicular to the coastline at rates of mm/yr. The transgressive deposits on the Eel margin exhibit marked variations in thickness alongshore; being thickest in the Eel River Syncline and thinnest over the Eureka Anticline. The divergent character of the infill in the syncline suggests that deposition is syntectonic. Fault displacement and structural relief observed along the transgressive surface are consistent with deformation rates measured onshore. The transgressive surface is offset ~0.5 m across the Eureka Anticline suggesting deformation has been active since ~10 ka. Two distinct acoustic units have been identified within the transgressive systems tract: a basal deposit that infills relief on the transgressive surface and an upper onlapping unit. The basal deposit infills lows along the outer shelf with a maximum thickness of 10 m and appears to be controlled by the early sea-level rise (21–7 ka) of the last deglaciation. It is separated from the overlying acoustically well-laminated unit by a pronounced surface of onlap. Moving shoreward along the inner shelf (<60 m water depth) the transgressive sequence thins and becomes acoustically transparent, which suggests that the finer-grained material is bypassing the inner shelf and being sequestered on the middle to outer shelf. It is here, on the inner shelf where tectonically induced accommodation exhibits the greatest control on sediment thickness. Thus, tectonics played a greater role when sea-level rise slowed after 7 ka to rates comparable to or slower than tectonic rates (~3 mm/yr). On the middle to outer shelf offshore of the Eel River, there is evidence for progradation and highstand deposition.

1. Introduction

The three independent variables of eustatic sea-level fluctuation, tectonic subsidence/uplift, and sediment supply control stratigraphic stacking patterns and associated facies (e.g., Sloss, 1963). Traditionally, tectonic subsidence or uplift is considered a modifier that tends to amplify or diminish the effects of eustatic sea-level changes (e.g., Posamentier and Vail, 1988; Posamentier et al., 1988). Indeed, along many passive margins tectonic deformation is usually characterized by thermal subsidence and sediment loading and the above assumption is valid. Nevertheless, along actively deforming regions, where the amplitude of the deformation is high (≥3 mm/yr) and the sign of the deformation changes along the margin (i.e., uplift/subsidence), tectonic deformation can impart a strong control on stratigraphic architecture (Driscoll and Hogg, 1995; Gerber et al., 2010). Here, we present new high-resolution seismic data acquired as part of the Office of Naval Research (ONR) STRATAFORM project that illustrate how the interplay between tectonic deformation, sediment supply, and sea level controls the architecture of transgressive deposits on an actively deforming margin. This paper focuses on the transgressive systems tract, highlighting its alongshore variability due to tectonic deformation.

In its simplest form, sequence stratigraphy predicts that a relative sea-level rise, or transgression, will form a thin, backstepping sequence due to a rapid increase in accommodation and shoreward migration of sediment supply (e.g., Vail et al., 1977; Van Wagoner et al., 1990; Christie-Blick and Driscoll, 1995). It is clear, however, that the geometry of transgressive deposits varies markedly depending on several factors such as preexisting slope of the shelf, oceanographic conditions, sediment supply, changing rates of sea-level rise, and local tectonic folding and faulting. For example, low gradient slopes favor rapid backstepping, while sediments on high gradient shelves

* Corresponding author at: Schlumberger Technology Corporation, 1325 S. Dairy Ashford Rd., Houston, TX 77077, USA. Tel.: +1 281 282 1505; fax: +1 281 285 1537.
E-mail addresses: lhogarth@slb.com (L.J. Hogarth), ndriscoll@ucsd.edu (N.W. Driscoll), jbabcock@ucsd.edu (J.M. Babcock), dorange@nikoindonesia.com (D.L. Orange).

0025-3227/$ – see front matter © 2012 Elsevier B.V. All rights reserved.
doi:10.1016/j.margeo.2012.02.005

have an increased likelihood of aggrading (Labaune et al., 2008). Variations in preexisting morphology will, therefore, create alongshore variability in TST thickness (e.g., Trincardi et al., 1994; Lobo et al., 2001). Oceanographic conditions can result in deposition of sediments away from their source (Driscoll and Karner, 1999; Labaune et al., 2008). Moreover, alongshore variability in sediment input or subsidence can result in the onset of progradation adjacent to a retrograding coastline (Catuneanu, 2006).

Along many margins, tectonic deformation and eustatic sea-level fluctuations operate in the same plane, that is, tectonic deformation constructively or destructively modifies eustasy with little along-strike variability (e.g., Posamentier and Allen, 1994; Jin and Chough, 1998; Labaune et al., 2008). In these scenarios, it is extremely difficult to tease out the tectonic signal from the eustatic signal (Christie-Blick and Driscoll, 1995). For example, in central California, researchers propose that tectonic uplift has interacted with eustatic sea-level rise to result in significant progradations during the postglacial transgression (Grossman et al., 2006). Likewise, Posamentier and Allen (1994) described the patterns of deposition in foreland basins and passive margins with a variation in subsidence rates that operated in the same plane as the sea-level changes.

On active margins such as the west coast of North America, tectonics plays an important role in generating morphology and subsequent stratigraphic architecture on the continental shelf (e.g., Orange, 1999; Burger et al., 2002; Hogarth et al., 2007; Le Dantec et al., 2010). Typically, rates of glacio-eustatic sea-level change exceed rates induced by local tectonic uplift or subsidence. In such cases, tectonic deformation plays a secondary role in creating observed sediment geometries. Nevertheless, during slower rates of sea-level change (<7 ka) tectonic deformation rates can equal or exceed rates of eustatic sea-level change, making it difficult to separate the signals. In areas where tectonic deformation is very localized (e.g., Gerber et al., 2010) or varies alongshore at high angles to eustatic changes (e.g., Hogarth et al., 2007; Le Dantec et al., 2010), the two signals are more readily identified and separated from one another. Such is the case on the Eel margin of northern California where E-W oriented forearc deformation is overprinted by N–S deformation due to the encroachment of the Mendocino Triple Junction (Clarke and Carver, 1992) and the Sierra Nevada Block (Unruh et al., 2003). This results in a variable signal of uplift and subsidence alongshore. In this study, we present new insights into the stratigraphic architecture generated on a tectonically active shelf during the most recent post-glacial transgression.

2. Regional setting

2.1. Geology

The Eel River forearc basin formed in the Neogene between the accretionary prism overlying the Cascadia subduction zone (CSZ) to the west and Cascade magmatic arc to the east (Fig. 1, inset; Clarke, 1992). Several episodes of deformation have occurred across the region since the Paleogene, with the last major episode of deformation occurring in the late Pleistocene. The Pacific ridge first subducted near Los Angeles ~30 Ma and resulted in the formation of the nascent San Andreas Fault (SAF), which has been migrating north and south in response to the cessation of subduction (Atwater, 1970; Atwater and Stock, 1998). Encroachment of the Pacific Plate and the northward migration of the SAF have imparted a north-northeast compression across the basin causing major folding and high-angle reverse and thrust faulting along north-northwest tends and reactivation of older north-trending fabrics. Since ~500 ka the encroachment of the Mendocino Triple Junction (MTJ), which is the northward propagating end of the SAF, has produced northeast-oriented shortening of at least 20 mm/yr (Clarke and Carver, 1992).

The Eel River Basin is segmented by rising anticlines that are underlain by active thrust faults (Figs. 1 and 2; Clarke, 1992). The northwest folds and faults are clearly imaged in the topography data and rotate away from the more north–south trending fabric approaching the MTJ (Fig. 1; McCrory, 2000; Gulick and Meltzer, 2002). The folds and faults are also imaged in offshore bathymetry and backscatter data with the anticline associated with the Little Salmon Fault (LSF) delineating the northern boundary of the large failure on the slope (Figs. 1 and 2).

In the study area at the southeast end of the offshore basin, several structures that appear to be rotated by the encroaching triple junction are oriented nearly perpendicular to shore (Figs. 2 and 3). The three main areas of uplift, from north to south, are the following: 1) Patrick's Point to the Mad River Fault Zone (MRFZ), 2) Eureka Anticline to Table Bluff Anticline, and 3) Centerville Beach to the Russ Fault. The intervening areas of subsidence are: 1) Freshwater Syncline, 2) the Little Salmon Fault, and 3) Eel River Syncline (Figs. 1 and 2; Vick, 1988). Vertical rates of motion on these structures range from 2.3 mm/yr uplift at Russ Fault to 3 mm/yr subsidence in the Eel River Syncline (Fig. 2). The most active structure is the LSF, which has been interpreted to be either (1) coincident with Table Bluff Anticline (McLaughlin et al., 2000) or (2) coincident with the south side of Humboldt Hill (Kelsey and Carver, 1988; Clarke, 1992) with the Table Bluff Fault Zone being an active branch of the LSF (McCrory, 2000). Onshore the LSF exhibits dip slip motion (McCrory, 2000; Gulick and Meltzer, 2002), but offshore in shallow water it records transpressive tectonics (Gulick and Meltzer, 2002). The slip rate on the LSF ranges from 4.6 ± 2.1 mm/yr estimated offshore (McCrory, 2000) to 6.1 ± 2.3 mm/yr estimated onshore (Clarke and Carver, 1992).

Continued deformation along the Eel margin is evidenced by earthquakes, uplifted marine terraces, and subsidence and flooding of peat horizons. Four depositional cycles of peat overlain by massive muds that gradually grade upward back into peats were observed in a 3 m core from the Mad River Slough (Vick, 1988). This pattern is interpreted to result from large earthquakes causing rapid subsidence (~2 m) followed by gradual refilling of the protected embayment. Radiocarbon dates of the horizons indicate a recurrence interval for these large earthquakes of 700–1000 years (Vick, 1988). Clarke and Carver (1992) also found evidence for late Holocene paleoseismicity on the LSF and in the MRFZ. They observed fault displacements of 1–4.5 m per event during the late Holocene and several other indicators such as uplifted driftwood and fossil mollusk shells as well as submerged and buried marshes and forests. They concluded that movements on the LSF and the MRFZ were associated with coseismic events on the CSZ megathrust, and future events could be up to $Mw = 9.5$ (Clarke and Carver, 1992).

2.2. Modern hydrodynamics and sediment dispersal

The Eel River, located in the south of the study area, has a compact drainage basin of 8640 km^2 consisting of rugged, easily erodable sedimentary and metamorphic terrain up to ~2000 m in elevation (Nittrouer, 1999). When combined with intense rainfall, the resulting suspended sediment to the coast yield is $\sim 2232 \times 10^3$ $kg/km^2/yr$. The smaller Mad River (1290 km^2) to the north has similar physiographic setting and a comparably large normalized sediment yield of $\sim 2070 \times 10^3$ $kg/km^2/yr$ (Wheatcroft and Sommerfield, 2005). Both rivers occupy subsiding synclines; the Eel River in the Eel River Syncline and the Mad River in the Freshwater Syncline (Fig. 2). The Eel River supplies the adjacent California margin with its largest total suspended sediment (TSS) load of 10–30 Mt/yr of silt and clay (Syvitski and Morehead, 1999), with ~25% of the river's TSS as fine sands (Sommerfield and Nittrouer, 1999), and ~10–20% of TSS as bedload (Brown and Ritter, 1971). The Eel River is a storm-dominated system with over 90% of its annual runoff occurring from November to May (Sommerfield and Nittrouer, 1999). Intense storms and large sediment discharge events are often coincident with energetic ocean conditions that act to redistribute earlier flood deposits over 10 cm in thickness, and transport ~80% of the silt and clay alongshore

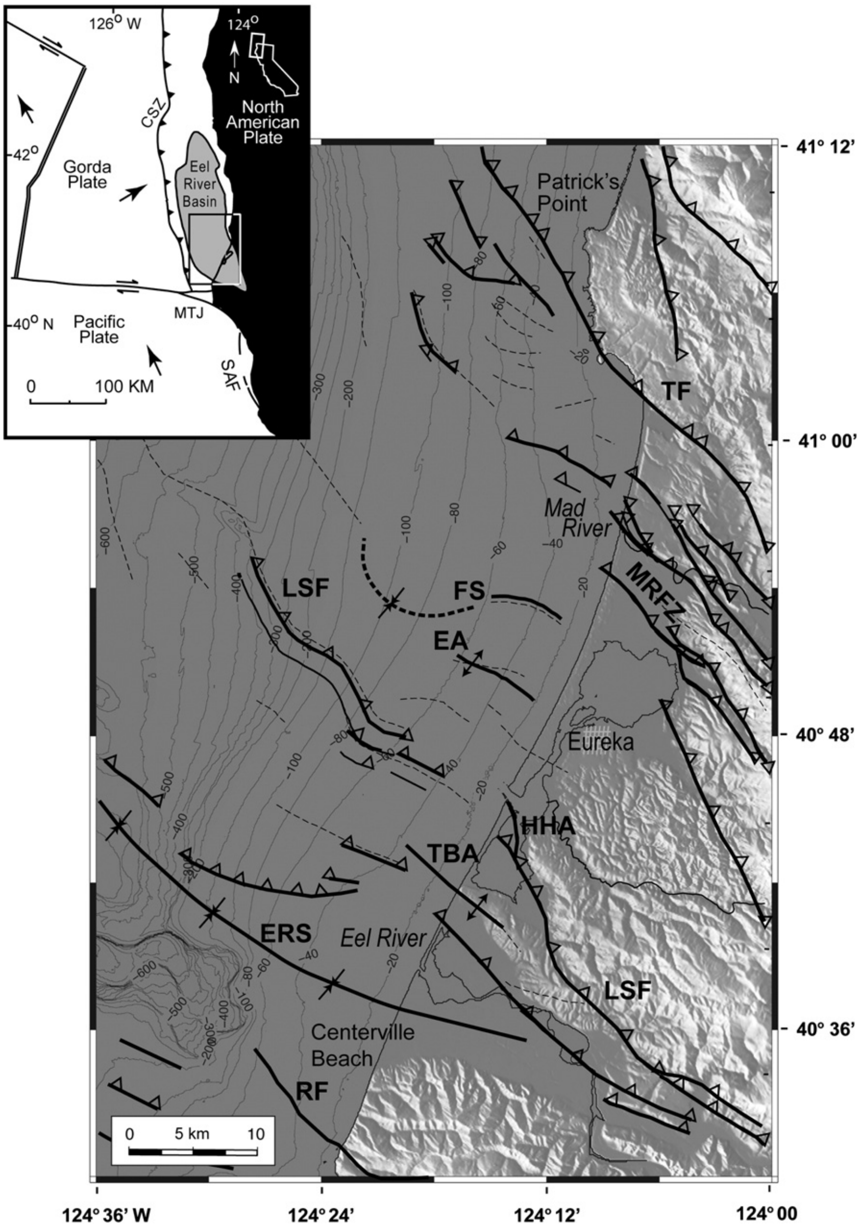

Fig. 1. Location map with local structural features and inset showing plate boundaries (after Clarke, 1992). Note that major local structures (black lines) are oriented at a higher angle to the coastline than the regional structures (e.g., San Andreas Fault [SAF], inset). These features include the Cascadia Subduction Zone (CSZ), Mendocino Triple Junction (MTJ), Russ Fault (RF), Eel River Syncline (ERS), Little Salmon Fault (LSF), Table Bluff Anticline (TBA), Humboldt Hill Anticline (HHA), Eureka Anticline (EA), Freshwater Syncline (FS), Mad River Fault Zone (MRFZ), Trinidad Fault (TF), and Patrick's Point (PP). Structures from Clarke (1992) and McLaughlin et al. (2000).

to the north and south (which may include offshore via the Eel Canyon) as well as to the outer shelf and slope (Wheatcroft et al., 1997; Alexander and Simoneau, 1999; Sommerfield and Nittrouer, 1999). Three characteristic sediment provinces are observed along the Eel margin: surficial sand facies grade from medium-grained sand on the beach to finer sand around the 50 m isobath; between ~50 and 60 m sand is interbedded with silt and clay; and in deeper waters silt and clay are dominant. Varying degrees and depths of biological mixing, accumulation rates, and original bed thickness across the shelf result in variable preservation potential of storm beds, with stratification being preserved on the central shelf, but not seaward of the 75 m isobath (Sommerfield and Nittrouer, 1999; Zhang et al., 1999). During the last 100 years, based on radiochemical (^{210}Pb) profiling, the maximum deposition occurred on the mid-shelf centered on the 70-m isobath (Sommerfield and Nittrouer, 1999). Modern sediment accumulation rates on the shelf vary spatially, with maximum accumulation rates an order of magnitude greater than the rates of tectonic deformation inferred from uplifted marine terraces (Vick, 1988; Orange, 1999).

3. Materials and methods

In 1998, 1999, and 2000 over 1000 km of CHIRP seismic data were acquired on the continental shelf offshore of the mouth of the Eel River as part of the STRATAFORM project (Fig. 3). Nearshore strike lines were collected in 1998 onboard the R/V Coral Sea, and regional dip lines were acquired in 1999 and 2000 onboard the R/V Thompson. The regional dip lines coincided with coring transects, for example, core Q45 coincides with dip line Q at 45 m water depth (Fig. 3). Vibracores, box cores, and piston cores collected across the study area provide information about the nature of facies and contacts observed in seismic data. We designed the cruise tracks to provide: (a) detailed

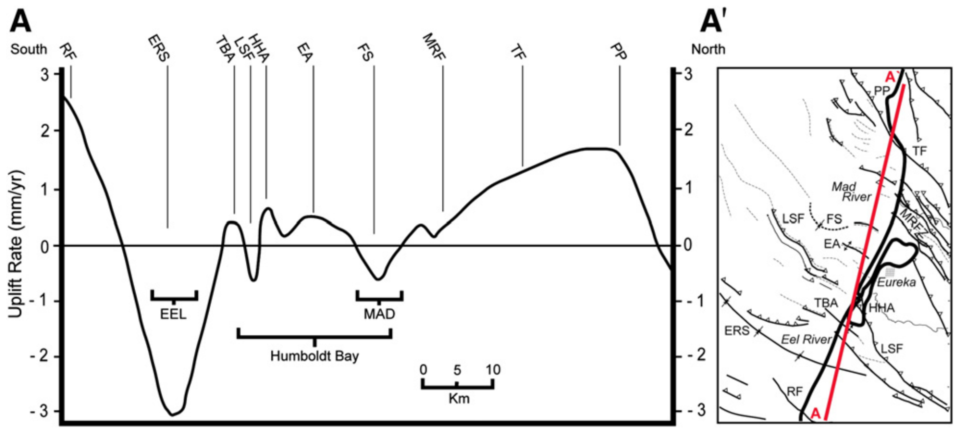

Fig. 2. Rates of uplift and subsidence along profile A–A' (see inset for location). Note the maximum rate of deformation of ~3 mm/yr occurs in the Eel River Syncline. Abbreviations are as labeled in Fig. 1. Modified after Vick (1988).

dip line coverage (~1.75 km line spacing) from the outer shelf/upper slope across the shelf into shallow water (~20 m) and (b) detailed strike line coverage (~250 m line spacing) of a prominent fold/fault system and overlying sediment thickness on the inner shelf. For the regional dip and strike lines a 1–5.5 kHz CHIRP signal with a 50 ms sweep was used, whereas for the nearshore surveys a 1–15 kHz CHIRP signal with a 10 ms sweep yielded improved vertical and horizontal resolution. These signals yielded submeter vertical resolution

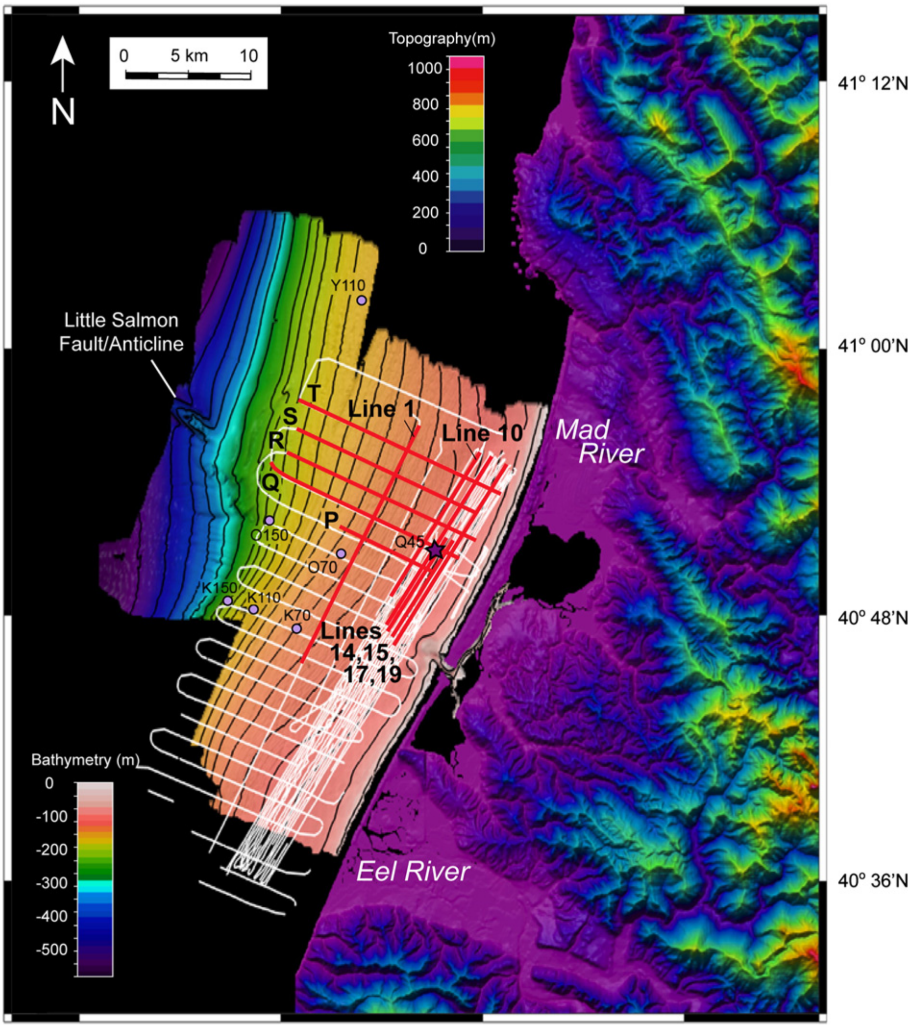

Fig. 3. Survey ship tracks superimposed on high-resolution bathymetry (Goff et al., 1999; Ferrini and Flood, 2002) collected as part of the STRATAFORM project. Contour intervals are: 10 m up to 100 m, 20 m up to 200 m, and 50 m up to 500 m depth. Red lines indicate profiles shown in Figs. 4, 5, 6, 7, and 11. Star indicates location of core Q45 shown in Fig. 10 and purple circles are the locations of cores referred to in the text from Sommerfield and Wheatcroft (2007). (For interpretation of the references to color in this figure legend, the reader is referred to the web version of this article.)

to subsurface depths up to ~50 m. Data were corrected for ship heave using SIOSEIS (Henkart, 2003) and further processed using Seismic Unix (Cohen and Stockwell, 1999). To correct for layback, one set of survey lines collected at one azimuth was held constant and the navigation for other lines was shifted to match the fixed lines. The total offset between lines (up to ~200 m) did not significantly impact correlation with structures onshore. Kingdom Software (Seismic Micro Technology www.seismicmicro.com) facilitated determining depths to interpreted surfaces as well as thickness of intervening units. We applied a nominal velocity of 1500 m/s to convert two way travel time to depth with both labeled on the seismic profiles. Generic Mapping Tools (GMT; gmt.soest.hawaii.edu/) were used to apply a continuous curvature surface algorithm and interior tension of 0.35 to convert data points to grid surfaces. Fledermaus software by Interactive Visualization Systems (IVS 3D, www.ivs3d.com) was used for three-dimensional perspective views.

A previous study in the region used both Huntec DTS reflection seismic data collected in 1995 and 1996 together with slightly lower resolution data acquired in 1977 and 1978 (Spinelli and Field, 2003). With a source bandwidth of 0.6–6 kHz the Huntec DTS system images slightly deeper (50–80 m) than the CHIRP system, but the vertical image resolution of the CHIRP is 1.5–2.5 times that of the Huntec DTS system. Furthermore, the higher resolution CHIRP seismic lines extend closer to shore than the Huntec DTS survey, and in nearshore sand-prone environments CHIRP resolution appears to be better than Huntec resolution (Baldwin et al, 2004; MARGINS 2004 Science Plans).

4. Results

4.1. Major structures and features

A strong subsurface reflector of regional extent marks an angular unconformity visible in inner shelf seismic sections (Figs. 4, 5, 6 and 7). The reflector exhibits much variability in roughness and acoustic character, being smooth with high acoustic amplitude in most areas, but rough with variable acoustic amplitudes in other regions, such as at ~75 m depth (Figs. 4, 5, and 6). In the southern half of the seismic survey area the angular unconformity is not well imaged, as gas-prone sediment prevented acoustic penetration deeper than ~30 m below the seafloor (Fig. 7D; Yun et al., 1999). Deposition above the reflector ranges from acoustically transparent to strong and parallel or irregular and wavy reflectors (e.g., Figs. 4, 5, and 6). Deposits below are also variable, transparent to strong reflectors, with wide (100 s of meters) and shallow (meters to 10s of meters) channel-like surfaces (Fig. 5), anticline structures (Figs. 6 and 7), and stacked, regularly-spaced reflectors. The overall topography of the angular unconformity in the northern half of the study area is marked by a broad high extending ~10–15 km along strike, adjacent to the MRFZ, the Freshwater Syncline, and the Eureka Anticline onshore (Fig. 1). In the northernmost dip lines the surface is covered by ~4–5 m of sediment at 40–50 m water depth (e.g., Line T; Fig. 4). Farther south, however, sediment cover decreases to a minimum of ~2 m over a nearly vertical fault and prominent anticline, which are well imaged in several lines (Figs. 6 and 7B), but are obscured by gas in other lines (Fig. 7A and C). The anticline and associated fault have been mapped by others, but are unnamed (Fig. 7; Clarke, 1992; McLaughlin et al., 2000). The trend of the fault/fold anticline within the structural high projects to the Eureka Anticline onshore, so we will refer to the anticline as the Eureka Anticline. Reflectors observed in the folded strata are parallel and are spaced at ~0.5–2 m. Strata of the south limb of the anticline dip toward the south at ~5–7° (assuming a vertical error of ±2 m and horizontal error of ±10 m). In strike line 15 N, the angular unconformity surface is visibly offset ~0.5 m across this structure (Figs. 7B and 8). Above the prominent reflector of the angular unconformity, at least one, and possibly two reflectors appear to be offset as well (Fig. 8 inset). To the south of the fault the truncation surface deepens and is covered by over 30 m of sediment (Fig. 7). A structure contour map of this prominent reflector shows that the trend of the distinct southern edge of a structural high is coincident with the offshore projection of the northern branch of the Little Salmon Fault, which coincides with the Humboldt Hill Anticline (HHA). We will refer to this entire suite of faults as the Little Salmon Fault Complex (LSF complex; Fig. 9). The LSF complex delineates the topographic high in the north from the structural low in the south and is outlined by the eastward deflection of the 60 m structure contour (Fig. 9). Within the southern low, we observe a local high adjacent to the Table Bluff Anticline (Fig. 9).

Sediments recovered in core Q45 were of sufficient depth to intersect the truncation surface at ~2 m depth, which correlates with a sharp erosive contact (Figs. 3, 5B, and 10). The contact separates fine-grained, laminated silt and clay below from a 75 cm-thick layer of coarse-grained, rounded pebbles and cobbles above (Fig. 10). Above the pebble and cobble layer, ~1 m of the core is rich in shell fragments.

4.2. Acoustic Unit I

We identify two distinct acoustic units above the regional unconformity. The lower unit, Unit I, directly overlies the strong reflector that marks the angular unconformity primarily at depths > 45 m. It is characterized by short, discontinuous, and strong to transparent reflectors (Figs. 4, 5, and 6). In regions overlain by Unit I, the angular unconformity appears to have more relief with a wavy acoustic character, appearing rougher than in areas where Unit I is absent (e.g., Fig. 6). Unit I thins shoreward by onlap (Figs. 4, 5, and 6). The Unit is most distinct in dip lines between ~60 and 100 m water depth and at shallower depths (~45–50 m) in strike lines directly to the south and north of the Eureka Anticline (Figs. 7 and 11). Although it thins seaward, it is unclear whether or not the unit pinches out at deeper depths as it both diminishes in acoustic reflectivity and is obscured by gas (Figs. 4 and 5). At deeper depths (90–120 m) there are a few subparallel reflectors within Unit I that dip less steeply than the transgressive surface (Figs. 4 and 5). In lines over the structural high (Lines Q and P) Unit I is thicker than to the north of the structural high (Line T). Furthermore, the acoustic character of Unit I exhibits concave-up, closely spaced (1–2 m), and truncated reflectors at shallower depths (60–90 m; Figs. 5, 6, and 11). Strike sections show that the unit infills topographic lows in the erosion surface, pinching out near the Eureka Anticline (Figs. 7 and 11). For example, in several strike lines to the north of the Eureka Anticline Unit I infills a broad low ~5 m deep that extends laterally ~2–3 km (Fig. 7). In strike sections, the onlap surface that forms the upper boundary of Unit I is smooth with a high-amplitude acoustic reflector (Fig. 7). The southern extent of Unit I is difficult to discern as gas obscures the subsurface reflectors (Fig. 7D).

4.3. Acoustic Unit II

Unit II is the uppermost sedimentary unit and is observed throughout the study area, but its acoustic character is highly variable. In dip lines at water depths > 60 m there are several parallel, high-amplitude, and largely continuous reflectors in Unit II, whereas nearshore areas are characterized by transparent sediment (Figs. 4, 5, 6, and 11). The acoustic reflectivity of the regional erosion surface increases coincidently with the increase in reflectivity of the overlying units. Some regions are obscured by high-amplitude reflections indicative of gas or fluid masking in the sediment (e.g., Figs. 6, 7C, and 7D). Note there are significantly fewer coherent reflectors observed toward the south in the Eel River Syncline (e.g., Fig. 7). In this region, Unit II has a blotchy, discontinuous acoustic character.

In line V, the northernmost dip line, which is located offshore of the mouth of the modern Mad River, Unit II sediments onlap Unit I,

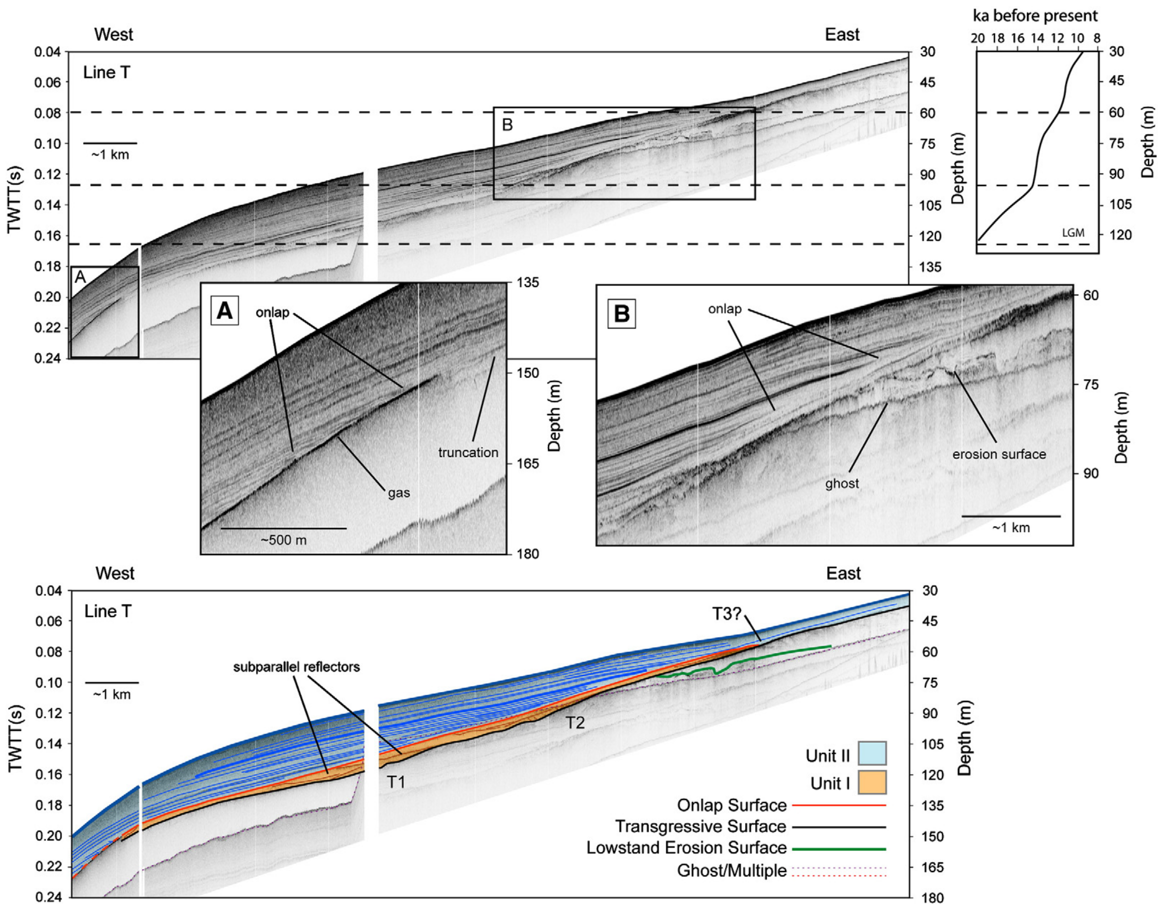

Fig. 4. Dip line T uninterpreted (top) and interpreted (bottom) crosses the margin just south of the Mad River and is adjacent to the subsurface structural high. The sea level curve to the right shows periods of slow sea level rise and is matched to the seismic profiles with dashed lines at depths corresponding to terraces (T1, T2, and T3). Inset A shows detail of the onlap surface between Units I and II at the shelf edge; inset B shows the onlap surface in the mid shelf and the lowstand erosion surface that is truncated by the transgressive surface. Vertical area in white on line T is a data gap.

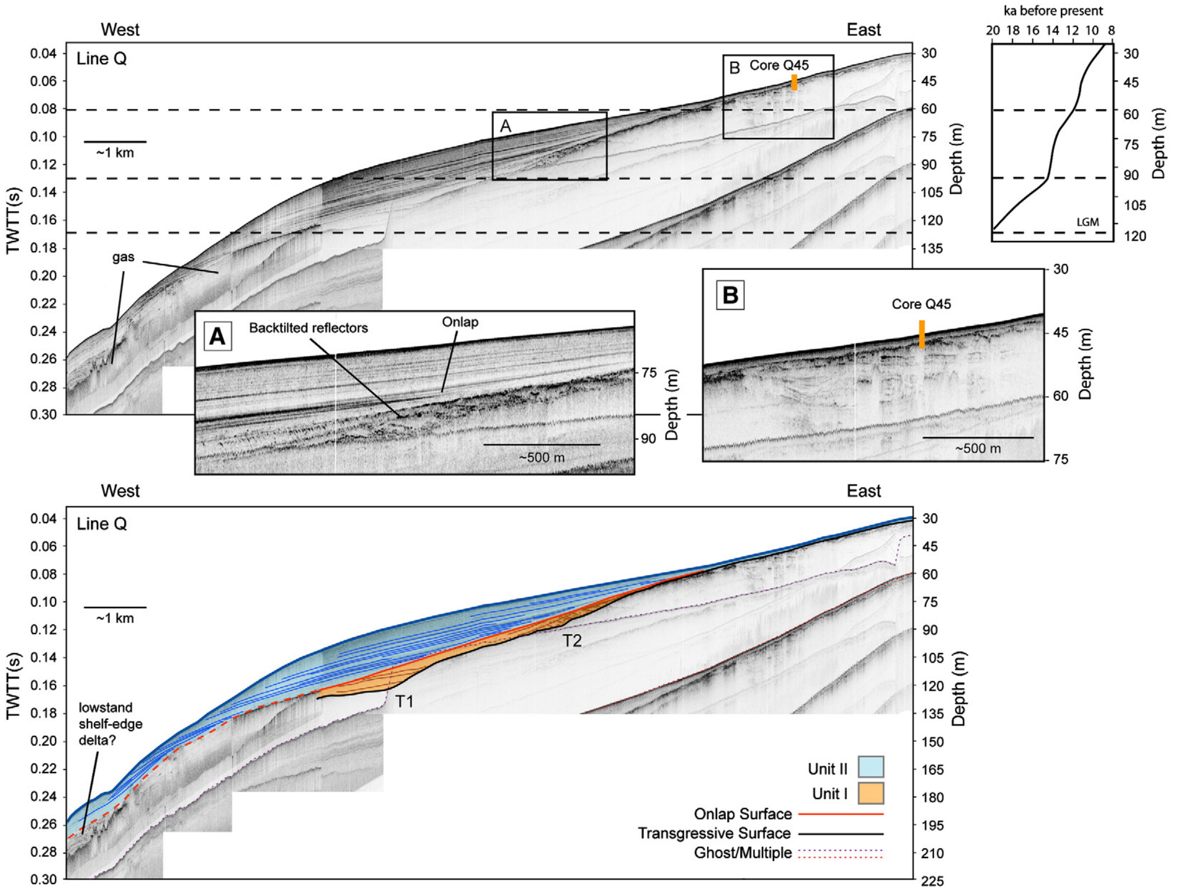

Fig. 5. Dip line Q uninterpreted (top) and interpreted (bottom) crosses the margin over the structural high associated with the Eureka Anticline. The sea level curve is as shown in Fig. 4. Inset A shows chaotic or backtilted reflectors within Unit I and the onlap of reflectors in Unit II. Inset B shows the approximate location of core Q45 (shown in Fig. 10).

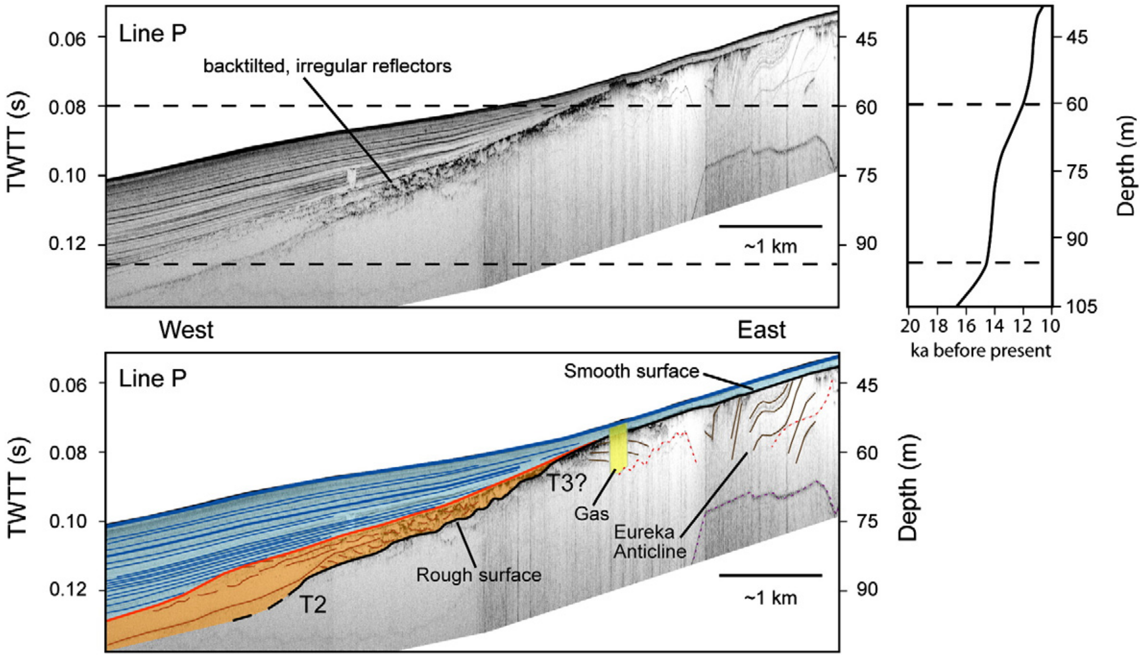

Fig. 6. Line P crosses the margin over the subsurface structural high directly over the Eureka Anticline. The sea level curve is as shown in Fig. 4, and horizon colors are the same as in Figs. 4 and 5.

thicken progressively from ~4 m at 30 m water depth to a maximum of ~25 m at 90 m water depth, and thin seaward. Immediately to the south, in line T, the thickness of Unit II is relatively uniform in the seismic section until ~60 m water depth where the sediments begin to thicken markedly seaward to a maximum thickness of ~25 m at ~80–90 m water depth (Figs. 4 and 11). Even though Unit II thins seaward from the 80 m isobath there is no observed downlap or shoreward migration of the downlap position in this region of the shelf, as might be expected at the distal edge of a prograding unit. Rather, the reflectors fade or perhaps terminate at the seafloor (Figs. 4 and 5). Farther south, Line Q, which overlies the structural high, exhibits very thin sediment cover above the transgressive surface (~1 m) to ~60 m water depth, with seaward thickening to a maximum (~25 m) at ~80–90 m water depth, and rapid thinning offshore (Fig. 5). In dip lines over the structural high, Unit II and the regional unconformity display the same characteristics observed in the lines to the north, that is, large lateral transition in acoustic amplitude of the erosion surface and variation from acoustically well-laminated reflectors along the outer and mid-shelf to an acoustically transparent unit on the inner shelf (e.g., Lines Q and P, Figs. 5 and 6).

Along strike, to the south, Unit II thickness increases towards the Eel River Syncline (Figs. 7 and 11), but the thickest part of the unit is not imaged because of gas occurrence that obscures reflectors from the underlying surfaces (Fig. 7D). The high amplitude horizons in Unit II onlap the inclined erosion surface as it dips into the Eel River Syncline. The onlapping reflectors exhibit divergence, and their dips systematically increase with depth to the south (Fig. 14).

4.4. Sediment isopach maps

An isopach map of Unit I shows that it is thin to absent over the structural highs, it has a maximum thickness of ~10 m to the west of the structural high in water depths of 60–100 m, and its distribution has linear trends parallel to the bathymetric contours (Fig. 12A). Across the margin, the unit thickens from 0 m around 60–70 m water depth to 10 m at ~90 m water depth and then thins offshore (Fig. 12A). The thickest deposits appear to correspond to the trend of the embayment delineated by the 100 m and shallower structural contours of the angular unconformity surface (Fig. 9). Abrupt changes in sediment thickness and depth to the regional erosion surface correlate with the trend of the LSF complex that separates a broad high to the north from a structural low to the south (Fig. 9).

The mid-shelf thickness maximum of Unit II is observed in dip lines at 80–90 m water depth (Figs. 12B and 12C). Although the structure map of the erosion surface shows little variation to the north of the LSF complex (Fig. 9), overlying sediments thicken gradually from ~1–2 m to ~5 m over a distance of ~10 km towards the Mad River Delta at water depths shallower than 60 m (Fig. 12B). The isopach maps also show the northeast margin of a sediment depocenter located to the south of the LSF complex (Fig. 12B and C). Within the area adjacent to the Eel River Syncline, where the regional erosion surface is locally high offshore of the Table Bluff Anticline, a sediment thickness minimum is observed in the nearshore (<30 m water depth; Fig. 12B). It is clear from the isopach map of Unit II that sediments are thinnest over the structural highs and thickest in the lows on the inner shelf (<60 m water depth; Fig. 12B).

In summary, the CHIRP data suggest that the late Pleistocene and Holocene succession on the Eel shelf is a seaward- and landward-thinning unit bounded by an underlying erosional surface and the overlying sea floor (Figs. 4, 5, 6, and 11). Unit I onlaps the erosional surface and Unit II onlaps onto Unit I, and these onlap positions have migrated landward through time. Across the shelf, this succession ranges from a few meters thick at the shelf break up to 35 m thick at the middle to outer shelf depocenter, thinning to less that 5 m at the 25 m isobath. Along the shelf, the thickness of the units exhibits marked variability, being thickest in the subsiding synclines (40+ m thickness), and thinning to less than 2 m across the axis of the Eureka Anticline (Figs. 7 and 12). The upper surface of the Holocene deposits slopes smoothly seaward and is poorly correlated with the relief on the underlying angular unconformity.

5. Discussion

5.1. Evolution of the transgressive systems tract

5.1.1. The transgressive surface

The shelf-wide unconformity that is characterized by truncation below and onlap above is interpreted to be the transgressive surface formed during the sea-level rise since the last glaciation (~21 ka-present). The transgressive surface is identified by a progressive shoreward shift of overlying facies (Christie-Blick and Driscoll, 1995). Both Units I and II exhibit such a backstepping character, which is indicative of a landward migration of sediment sources. As such, we interpret these two units as the transgressive systems tract. Nevertheless, constructional relief on the middle to outer shelf off the Eel River suggests that a portion of Unit II might be part of a

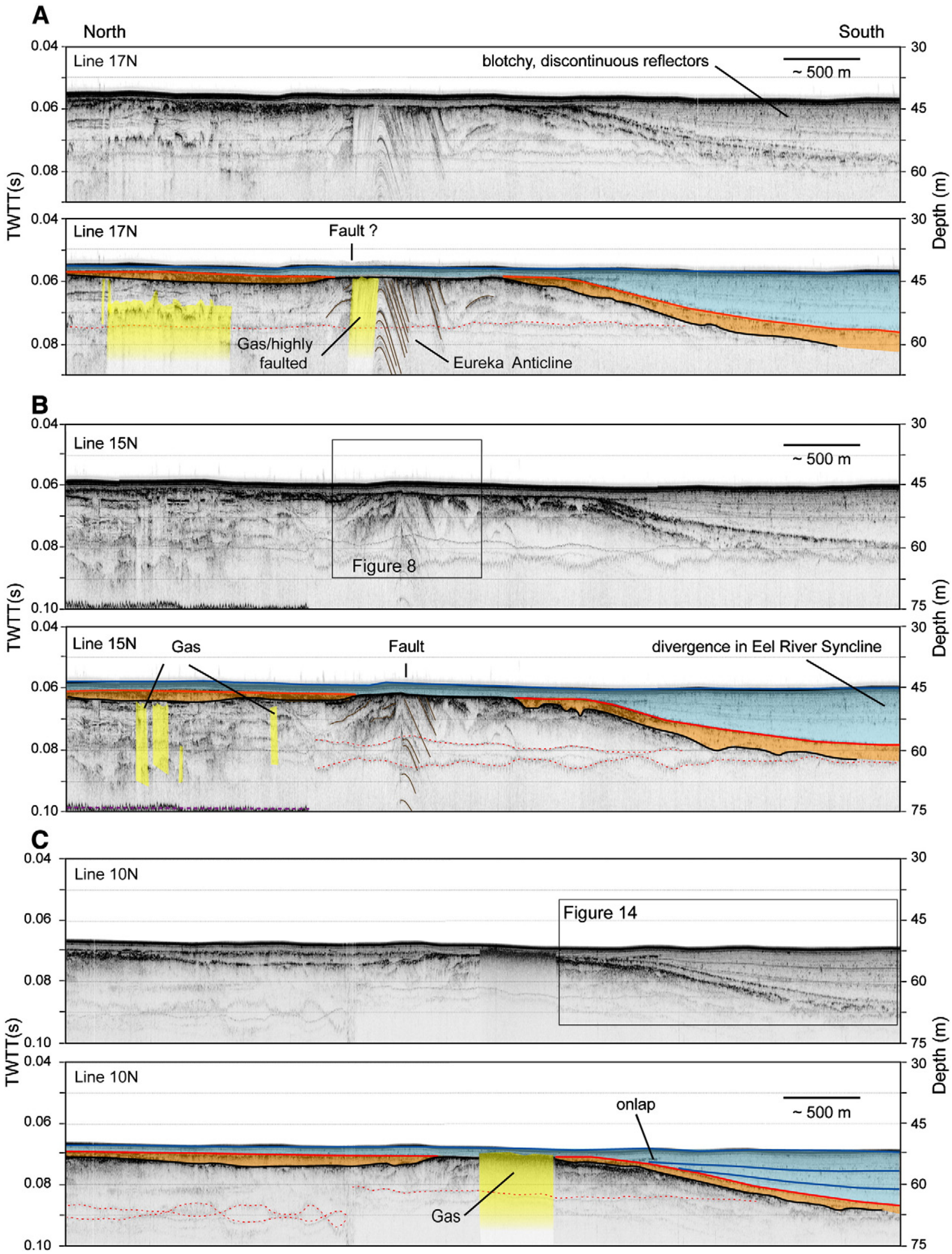

Fig. 7. Strike lines A: 17, B: 15, C: 10, and D: 1 uninterpreted (top) and interpreted (bottom). In strike lines the transgressive surface and a prominent anticline and fault are imaged. The transgressive surface deepens to the south towards the Eel River Syncline. Note reflectors are intermittently obscured by gas throughout much of the study area. D shows the predominance of gas within the ERS and the location of cores O70 and K70. Color scheme is same as shown in Fig. 4.

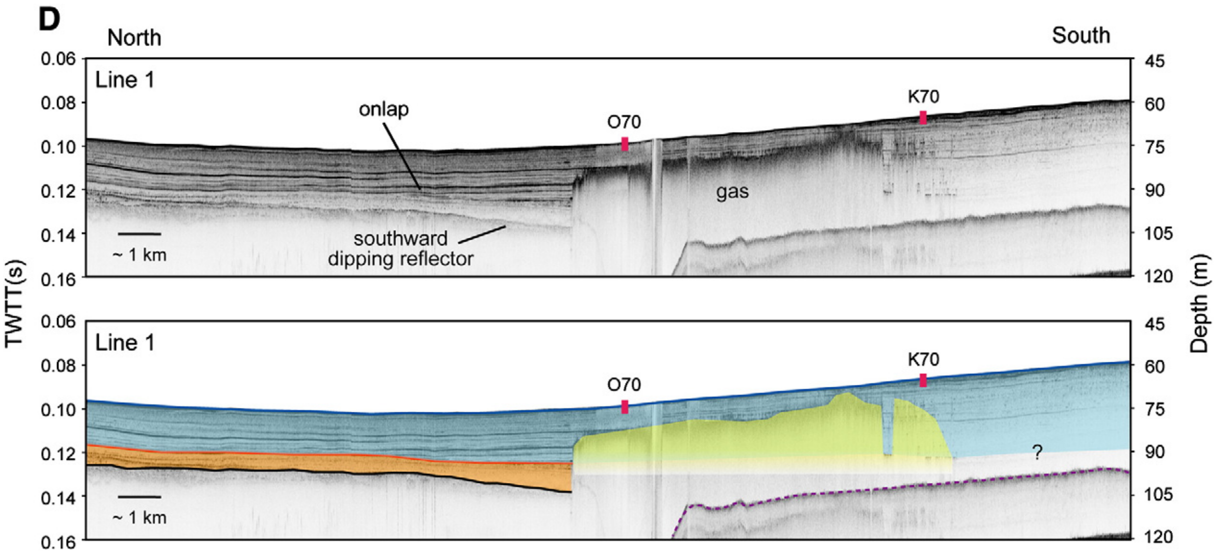

Fig. 7 (*continued*).

highstand systems tract as the margin is prograding seaward. The widespread gas in this region prohibits accurately identifying the downlap surface associated with this progradation.

The geometry of the shelf-wide unconformity also supports our identification of the transgressive surface. The surface exhibits three subtle steps or terraces at ~125 m (T1), ~100–90 m (T2), and ~60 m (T3) depth (Figs. 4, 5, and 6). We propose that these low areas correspond with periods of slow sea-level rise during the early deglaciation. The terrace at T1 corresponds to the sea level of the LGM (21–20 ka), T2 corresponds to period of slow sea-level rise preceding meltwater pulse 1A (~14 ka; Bard et al., 1996), and the depth of T3 corresponds to the slow sea-level rise prior to meltwater pulse 1B (~11.3 ka; Bard et al., 1996; Fig. 13). Wave-cut terraces and shoreline notches are formed when the rate of sea-level rise is low. Conversely, during rapid rises associated with meltwater pulses pre-existing shelf

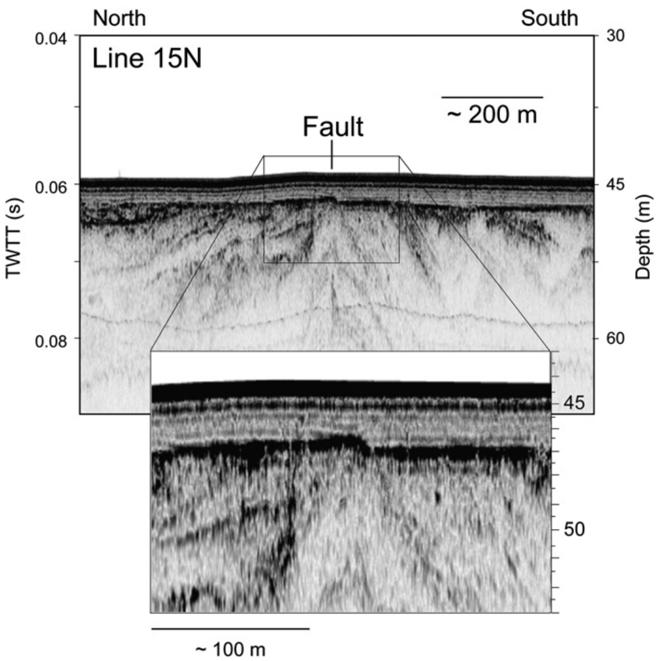

Fig. 8. Detail of strike line 15 showing fault offset in the transgressive surface above the Eureka Anticline. See Fig. 7 for location.

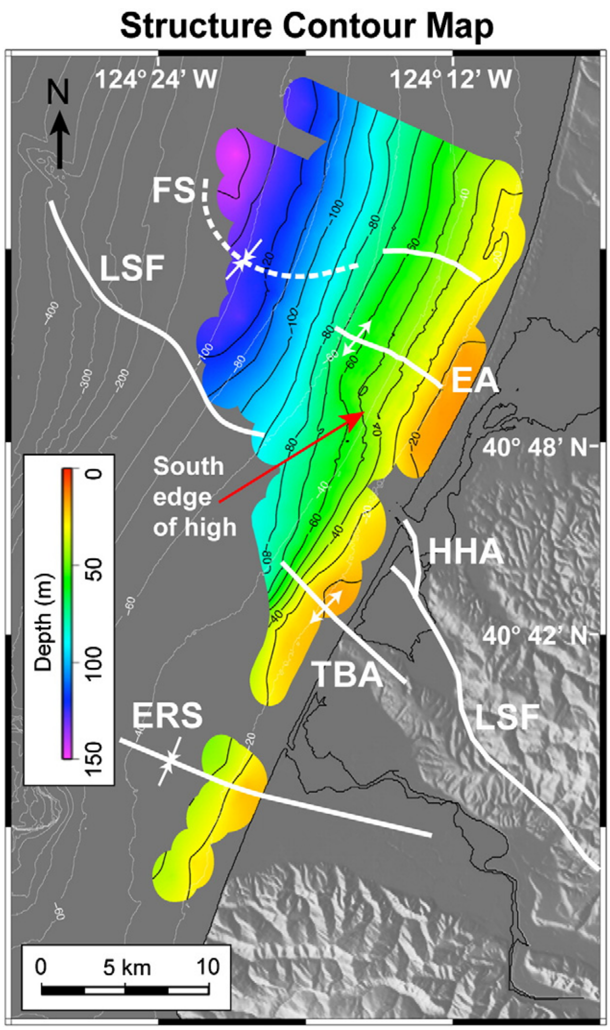

Fig. 9. Structure contour map of the depth to the transgressive surface shows the abrupt eastward jog and deepening to the south of the northern high and a slight high offshore of the Table Bluff Anticline. Selected tectonic features are superimposed in white with the same abbreviations as in Fig. 1.

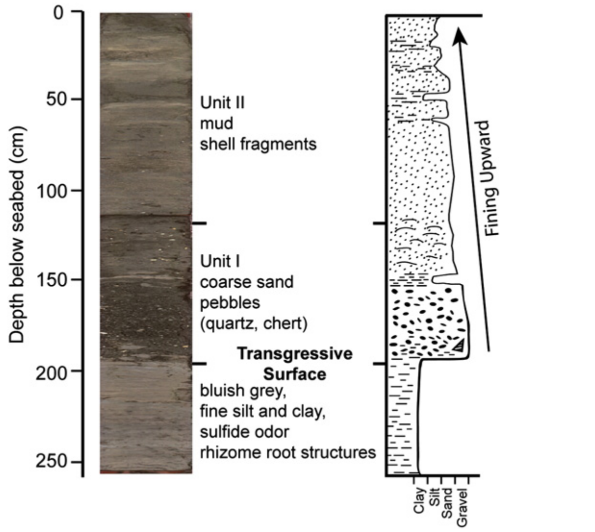

Fig. 10. Core Q45 recovered the transgressive surface, which separates transgressive marine deposits above from subaerial deposits below. Note the coarse-grained lag deposit associated with the transgressive surface, the subsequent fining upward, and the marked difference between the upper and lower fine-grained units. See Figs. 3, 5, and 11 for core location.

morphology is preferentially preserved. These wave-cut terraces resemble the “steps” detailed by Grossman et al. (2006) in the transgressive surface offshore of Santa Cruz, CA.

5.1.2. Unit I

We interpret Unit I, which is bounded by the transgressive surface below and by a flooding surface characterized by backstepping, onlapping reflectors above, as a transgressive lag deposit. Our interpretation of this unit is based on its aerial and stratigraphic location as well as its acoustic character, sedimentary geometry, and core data. Unit I is thickest in water depths > 60 m, with the thickest deposits roughly following shore-parallel trends to the west of a structural high that is bounded on its southern edge by the LSF complex (Fig. 12A). In seismic profiles, Unit I occupies a broad (~10 km across the shelf) low area in the transgressive surface seaward of the 60 m isobath (Figs. 4, 5, and 6). Within this structural low, we observe the three terraces described above (T1, T2, and T3). The terraces and shoreline notches control the thickness of Unit I and impart the stepped shore-parallel trend observed in its isopach map (Fig. 12A).

Periods of slow sea-level rise during the transgression allowed for localized erosion with the formation of terraces and notches. These erosional features were subsequently filled by sediment eroded from nearshore regions when sea level was higher. For example, after T2 was eroded and sea level reached T3, sediments eroded from this shoreline were transported offshore where they infilled and obscured the underlying roughness on the transgressive surface at T2. The thin veneer of coarse-grained, rounded pebbles and cobbles immediately overlying the transgressive surface in core Q45 reflects a high energy environment and the coarse-grained sediment lag that would be deposited under the influence of waves just offshore of the beach and surf zone (Fig. 10).

It is possible that the sediments of Unit I are estuarine in nature and were deposited during early sea-level rise shoreward of the beach, as

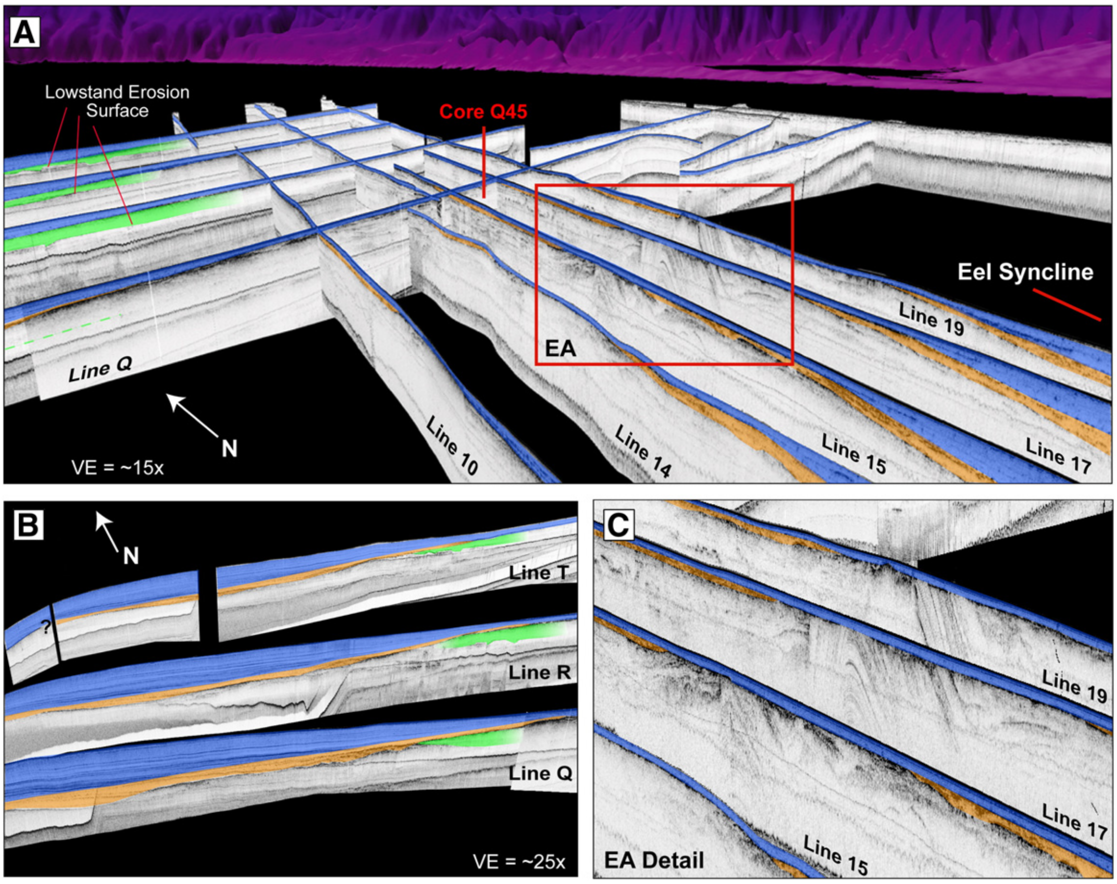

Fig. 11. A: Perspective view showing strike and dip lines on the edge of the structural high with Unit I (orange) confined mostly to its flanks and Unit II (blue) thickening into the Eel River Syncline and offshore. B: Perspective view showing the thickest deposits of Unit I on the west side of the structural high, the unit thins both landward and seaward, and truncates the underlying lowstand deposits (green). C: Detailed view from (A) showing the Eureka Anticline (EA). (For interpretation of the references to color in this figure legend, the reader is referred to the web version of this article.)

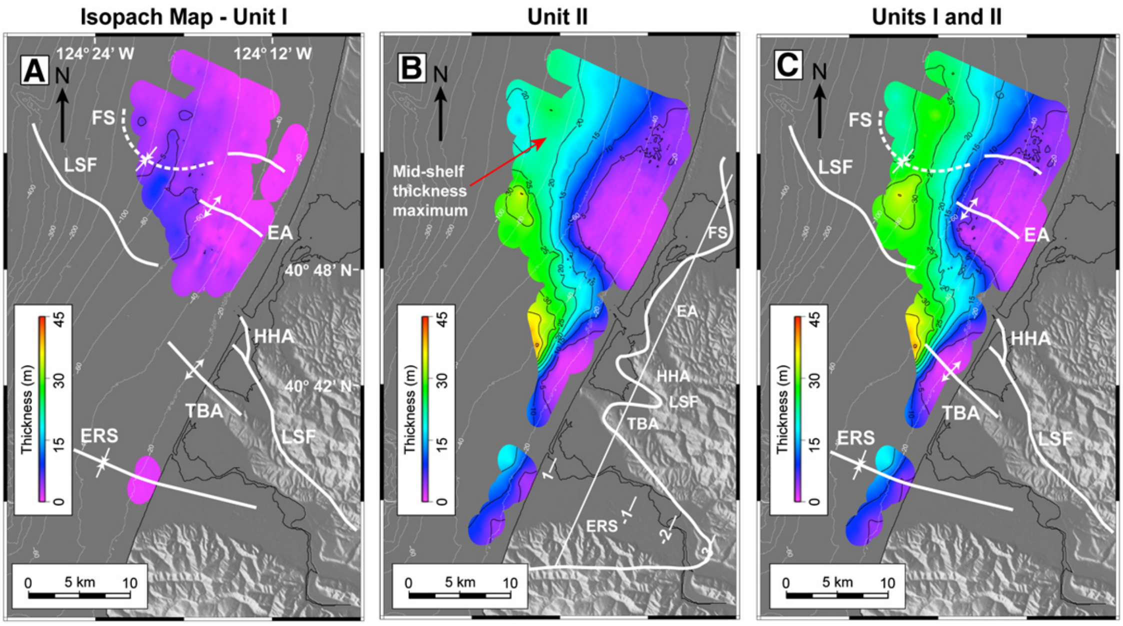

Fig. 12. Isopach maps. A: Unit, I B: Unit II, and C: Units I and II. In (A) and (C) selected tectonic features are superimposed in white, and in (B) uplift and subsidence rates onshore are superimposed in white with the same abbreviations as in Fig. 1. Contour interval is 5 m.

hinted at by Spinelli and Field (2003), but the location of the sediments does not correspond with their proposed Mad River source. The observed backtilted and chaotic character observed between 75 and 90 m depth could represent a backbarrier beach environment (e.g., Havholm et al., 2004), but it is unlikely that shoreface deposits would survive the extremely high wave energy of this environment during transgression. Therefore, we interpret these chaotic deposits as coarse grained sediments derived from local wave-base erosion, and the liberated material is moved offshore where it preferentially infills previous wave-cut terraces (e.g., T1; Fig. 5).

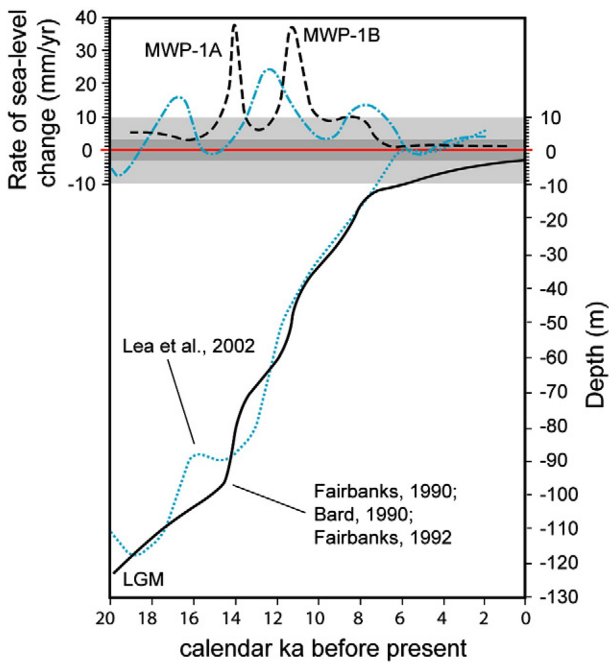

Fig. 13. Sea-level curves based on Lea et al. (2002) in dotted blue and Bard et al. (1990), Fairbanks (1990), and Fairbanks (1992) in solid black. Rates of sea-level change are shown at the top in corresponding colors. Note the scale for rates of sea-level change are shown on the left in mm/yr and depths are shown on the right in meters. Maximum rates of tectonic deformation are shown in gray (±10 mm/yr; e.g., Brothers et al., 2009).

The seaward extent of Unit I is not well imaged due to gas wipeout at depth (125–145 m) near the shelf edge. The onlap along the outer shelf could be interpreted as a lowstand shelf edge delta deposit (Figs. 4 and 5). Nevertheless, without core data, it is difficult to tell if the unit is coarse grained or fine grained. This has implications for the origin of the deposit either being a lowstand shelf edge delta or possibly a healing phase deposit formed during the transgression (Posamentier and Allen, 1993; Catuneanu, 2006).

5.1.3. Unit II

Based on sediment thickness, distribution, acoustic character, and core data we interpret Unit II as primarily marine transgressive deposits. The flat, laminated nature of sediments in Unit II deeper than ~50 m water depth and the fine-grained (mud) sediments recovered in cores indicate Unit II was formed by deposition along an open shelf. On the inner shelf, the transparent acoustic character of Unit II and cores from the upper 1–2 m (Sommerfield and Nittrouer, 1999) show homogenous sands with little to no acoustic impedance contrasts. These patterns suggest ephemeral nearshore deposits are reworked, transported offshore, and sequestered on the mid to outer shelf or transported beyond the shelf edge, which is consistent with recent modeling work by Fan, et al. (2004).

The onlapping, backstepping character of Unit II at depths > 50 m indicates shoreward migration of the coastline and sediment source during transgression. Along strike, Unit II shows marked divergence in the Eel River Syncline with the dip of each reflector increasing with depth (Figs. 7 and 14). The thickness variations of Unit II are as large, if not larger, along the margin as they are across the margin (Fig. 12B); the thickness ranges from > 40 m in the subsiding Eel River Syncline to < 2 m across the axis of the Eureka Anticline. Previous research shows that post-glacial sediments could be 50–60 m thick in the syncline (Spinelli and Field, 2003). Fig. 11 illustrates the three-dimensional onlap pattern; Unit II onlaps the transgressive surface toward the east and toward the north on the northern limb of the Eel River Syncline.

The thickness of this deposit led Burger et al. (2002) to assign it to the highstand systems tract. Although individual parasequences within a given systems tract can exhibit both backstepping and prograding geometries, the depositional systems tracts are defined primarily by their architecture and facies associations (Posamentier and Vail,

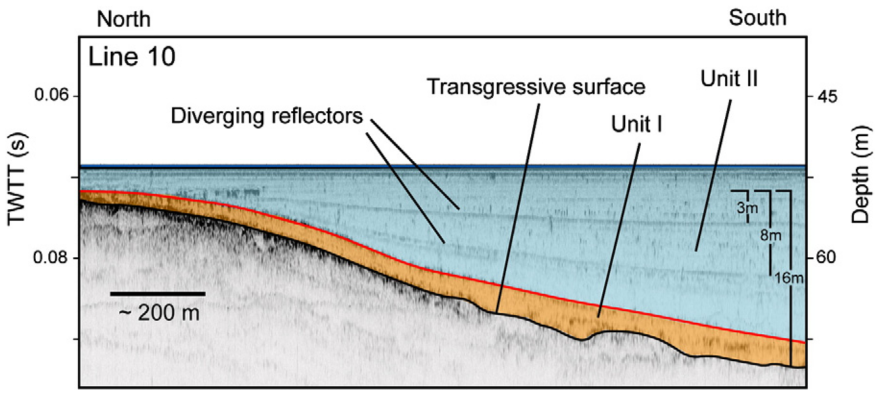

Fig. 14. Enlargement of strike line 10 showing divergence of reflectors into the Eel River Syncline. In addition, depths to the transgressive surface and reflectors within Unit II are shown for the deformation rate derived in Section 5.2.2. See Figs. 3 and 7C for location.

1988). A transgressive systems tract is composed of backstepping beds, which terminate landward by onlap and seaward by downlap. The highstand systems tract is composed of offlapping beds with downlapping seaward terminations that evolve from aggradational to progradational in response to available accommodation. The surface between the two tracts, known as the maximum flooding surface (Swift et al., 1991), separates discordant sets of bedding planes. As the majority of these sediments (up to ~50 m depth) exhibit a shoreward shift in onlap and there is no evidence of progradation, the bulk of the deposits above the transgressive surface on the Eel shelf must be assigned to the transgressive systems tract.

5.1.4. Highstand

Although there is no observed stratigraphic evidence of highstand deposition such as a downlap surface and progradation, there is geomorphic evidence of incipient highstand deposits. At water depths < ~55 m Unit II is transparent and lacks reflectors (Figs. 4, 5, and 6). Therefore, the upper ~2 m of sediment on top of the structural high (Figs. 4, 5, 6, and 7) could be highstand deposits. It is also clear from the geometry of reflectors within Unit II that the sediment is aggrading on the mid to outer shelf within the ERS (Fig. 7D). The geomorphic expression of the Eel River delta is evident in the 40 m and 60 m isobaths, which are deflected seaward (Fig. 1). According to other researchers, a coastal plain has developed since the late Holocene reduction in the rate of sea-level rise, and as of ~5 ka the Mad and Eel estuaries have inverted as deltas (Goff et al, 1999; O'Shea, 2005). Note, however, that the 20 m isobath parallels the shoreline (Fig. 1), and shallow strike lines show little shoaling of the seafloor (Fig. 7A–C), whereas deeper strike lines exhibit significant shoaling adjacent to the Eel River sediment source (Fig. 7D). The deformation associated with the ERS observed at depth is infilled and obscured by onlapping sediments with no evidence of deformation up section (Fig. 7D). This observation suggests that the deformation associated with the ERS dies away offshore toward the west. Thus, the geomorphic expression of highstand deltas is only evident in the mid to outer shelf. Conversely, Humboldt Bay, which is coincident with the broad structural high offshore, exhibits the characteristics of a transgressive coastline (barrier islands, estuaries) and may still be experiencing transgression.

5.2. Controls on sediment thickness

5.2.1. Eustasy

The 125 m shift in sea level since the last glacial maximum (~21 ka) has played a major role in the formation of the architecture of the Eel margin. During the early Transgression (21–7 ka, Fig. 13) eustasy was the dominant driver of deposition as flooding of the outer shelf occurred during this time. Intermittent periods of slow rise carved terraces, which later filled with sediments of Unit I. As sea-level rise slowed (~7 ka), tectonic deformation along the margin started to play a larger role in controlling accommodation along the margin (Fig. 13).

The distribution and thickness of Unit I is largely a result of eustasy, as the unit coincides with the location of negative relief along the transgressive surface (Figs. 4, 5, and 7). These topographic lows likely resulted from enhanced erosion during slow sea-level rise as opposed to a structural low associated with the Freshwater Syncline as proposed by Spinelli and Field (2003). The isopach map shows that Unit I is thickest along the edges of the broad structural high delineated on its southern edge by the LSF complex (Fig. 12A). There is no evidence in the seismic data of a structural control associated with the Freshwater Syncline (Figs. 9 and 12A) as proposed by Spinelli and Field (2003). Rather, the depocenter exhibits a shore-parallel trend and cuts across the trend of the Freshwater Syncline (Fig. 12). Furthermore, evidence from Burger et al. (2002) shows that the Freshwater Syncline has been inactive since ~500 ka and overlying units are generally flat lying with little to no evidence of deformation. Evidence of erosion (and non-deposition) suggests that the Eureka Anticline and adjacent shoal were a structural high throughout the last sea-level rise. At lower stands of sea level, given the geometry of the Eureka Anticline and adjacent region, the shoreline would have taken an abrupt eastward jog along its south end (Figs. 9 and 12). Thus, as sea level transgressed across this shoreline, sediments would have been shunted both to the northwest, west, and southwest of the high, consistent with our observations (Figs. 9 and 12). Unit I transgressive deposits are thickest to the west of the structural high and thin along the edges, which may reflect the tendency for aggradation along a steep slope rather than retrogradation along the more shallowly sloping edges of the high (Labaune et al., 2008).

5.2.2. Tectonics

At shallow depths (<60 m), the thickness of the transgressive sequence is predominantly controlled by the along-shore variation in tectonic deformation due to folding in the region (Figs. 1, 2, and 11). Sediment is preferentially deposited in lows where expanded sections are observed. This pattern represents the long-term sediment accumulation controlled by tectonically generated accommodation. As few of the cores acquired during STRATAFORM penetrated the transgressive surface (O'Shea, 2005), we have examined the stratal patterns and onshore paleoseismic work to place some constraints on the relative timing of deformation. Vertical offset of the transgressive surface over the Eureka Anticline (Fig. 8) indicates coseismic displacement of ~0.5–1 m since sea level transgressed that water depth (~50 m). Assuming wave-base erosion reworked the shoreface and subsequent deformation offset that planar surface, deformation on the Eureka Anticline has occurred since ~10 ka (Fig. 13). Activity on the Eureka Anticline is consistent with mid-Pleistocene to Holocene activity inferred on the nearby LSF, MRFZ, and Table Bluff Anticline by other researchers (Clarke and Carver, 1992; McCrory, 2000; Gulick and Meltzer, 2002).

The high sediment input to the margin provides a high fidelity record of deformation afforded by diverging, highly reflective horizons within Unit II (Figs. 7 and 14). The divergence of bedding in Unit II with increasing distance away from the LSF complex records the uplift along the fault combined with subsidence in the Eel River Syncline of up to 3 mm/yr (Fig. 2; Vick, 1988). The divergent geometry of the reflectors in the Eel River Syncline indicates that deformation has been ongoing (Fig. 15A and B) rather than predating deposition (Fig. 15C). Although the geometry we observe is more like case A in Fig. 15, the high-amplitude reflectors in Unit II, which are interpreted to represent time-synchronous event horizons, may not occur with sufficient frequency to determine whether deformation is continuous (Fig. 15A) or episodic (Fig. 15B). The former is possible, but based on previous researchers' observations of episodic events on the LSF (e.g., Vick, 1988; Clarke and Carver, 1992) it is more likely that deformation

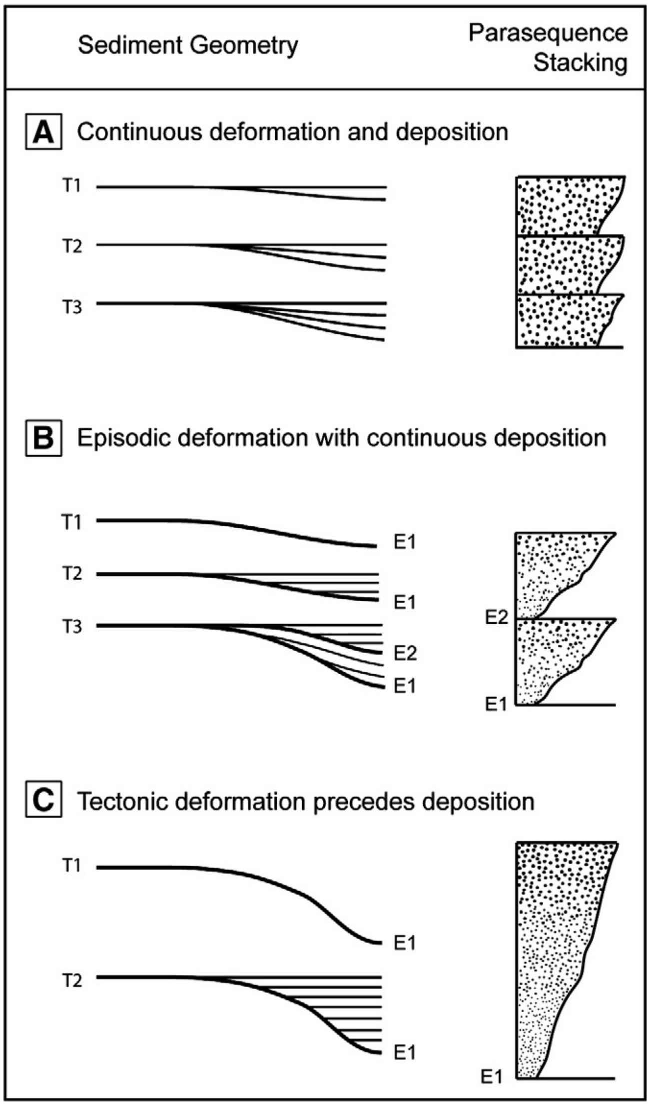

Fig. 15. Predicted stratigraphic geometry and parasequence stacking for three possible scenarios of deformation and sedimentation. A: Synchronous and ongoing deformation and sedimentation would result in little change in grain size going up section; B: highly episodic deformation coupled with continuous sedimentation would result in a series of stacked, coarsening upward packages; and C: when all deformation predates sedimentation an overall coarsening upward pattern would be expected. Deformation events (e.g., E1) and time periods (e.g., T1) are shown.

offshore has also been episodic. Karner et al. (1993) observe geometry much like case B in Fig. 15, where diverging angular unconformities mark episodic deformation events in the Central Indian Ocean (see their Fig. 8). Therefore, we assume the episodes of deformation have been relatively regular in the ERS.

Long cores are needed to provide more insight into the nature of the deformation. We predict that continuous deformation and sedimentation would result in very little grain-size change throughout the core (Fig. 15A), but episodic deformation, which would create rapid deepening, and would result in a pattern of recurrent, coarsening upward units (Fig. 15B). Alternatively, flat-lying geometry and an overall coarsening upward package would be observed if deformation preceded deposition (Fig. 15C). Unfortunately cores from the STRATAFORM project did not sample deeper than ~3–5 m below the seafloor on the shelf and thus were not able to define the grain size patterns or date the reflective horizons observed in the ERS (Fig. 11).

Although we do not image the thickest deposits within the ERS we can estimate deformation rates at the northern end of the syncline. The thickness of Unit II sediments in line 10 represents ~1.4 ± 0.3 mm/yr of deformation assuming an age of 11.5 ± 0.5 ka for the transgressive surface in that location and a sound speed of 1500 ± 50 m/s (Fig. 14). Given this estimate of the deformation rate is along the northern side of the ERS, naturally it would be lower than the maximum rate at the fold axis of the syncline of ~3 mm/yr observed onshore (Fig. 2; Vick, 1988). The accommodation in this region is predominantly due to tectonic deformation during the latter part of the postglacial sea-level rise. That is, from ~21 to 7 ka rates of sea level rise were high (up to ~40 mm/yr; Fig. 13), but as sea-level rise slowed (7 ka-present) rates of tectonic deformation in the ERS matched or exceeded rates of sea-level rise (Fig. 13). Thus, during the late postglacial, along-strike changes in accommodation appear to be largely controlled by tectonic deformation.

5.2.3. Hydrodynamics and sediment source

Rapid sediment accumulation in the structural lows masks the tectonically induced relief along the Eel margin. This superimposition of sediment source and tectonic deformation results in a poor correlation between the relief on the seafloor and that on the underlying transgressive surface (Figs. 1, 3, and 9). As expected with diminished rate of sea-level rise and high sediment input, accommodation has been filled or exceeded on the shelf adjacent to the Mad and Eel Rivers where sediment thicknesses are greater than that observed across the intervening structural high. Although sediment thickness in the ERS is largely controlled by tectonic deformation, bathymetry and strike lines that parallel the shoreline show that there is excess sediment accumulation as part of a subaqueous delta, and it has deflected the 40 m isobath seaward in front of the Eel River mouth (Figs. 1 and 3). A similar observation appears to hold offshore of the Mad River, but our survey coverage did not extend far enough north to adequately document this trend.

Radiocarbon dates reported by Sommerfield and Wheatcroft (2007) from cores collected as part of the STRATAFORM project give insight into the rates of sediment accumulation across the shelf for the late Holocene. Rapid sedimentation has occurred in the ERS, where sediment accumulated at 5.9 mm/yr over the past 1500 years in core K70 (Fig. 3). This location is roughly coincident with the maximum depocenter of transgressive sediment mapped by Spinelli and Field (2003). On the southern edge of the broad structural high associated with the Eureka Anticline, sedimentation was slower at 2 mm/yr over the past 2500 years. Shelf edge deposition ranged from 0.2–0.3 mm/yr (O-150 and K-150) at 150 m water depth to 1.2–2.5 mm/yr (Y-110 and K-110) at 110 m water depth (Fig. 3). Sommerfield and Wheatcroft (2007) attribute this variation in sedimentation rates to ongoing creation of accommodation in the ERS, which allows high rates of accumulation, while sediment is transported off of the structural highs. While sea-level rise and variation in tectonically induced accommodation clearly govern the longer term (5–20 kyr) sediment thickness pattern, the location of the sediment source appears to govern the modern sediment deposition on the mid to outer shelf reflected by accumulation rates in these cores. Interestingly, although reflectors in Unit II diverge and deepen in the inner shelf, the seismic lines from the mid to outer shelf show that the upper sediments are flat lying or even aggrade across the Eel River Syncline (Fig. 7D). The change in character from southward dipping to flat lying as one moves offshore indicates that deformation in the ERS diminishes offshore and may have ceased.

The mid-shelf wedge visible between ~80 and 90 m of water depth in the Eel River Basin is likely the result of hydrodynamic conditions such as wave climate and the currents that carry Eel River storm sediments to the north (e.g., Sommerfield and Nittrouer, 1999; Harris et al., 2005). The location of the depocenter on the outer shelf at 80–90 m water depth is deeper than the water depth of the depocenter observed by studies of sediments deposition on time scales of 100 s of years (centered ~70 m; Sommerfield and Nittrouer, 1999). This shoreward offset is most likely temporal, and with continued exposure to storm activity and reworking the short-term depocenter will eventually be transported offshore.

6. Conclusions

Analysis of high-resolution CHIRP data provided a detailed view of surficial sediment architecture and illuminated the different controls on sediment deposition and preservation on the shelf since the Last Glacial Maximum (~21 ka). The transgressive systems tract of the Eel River shelf is composed of two acoustic units, a deposit that infills relief along the transgressive surface and an upper transgressive unit of aggrading, backstepping marine deposits. Sea-level rise controlled the distribution of sediment during the rapid rise from ~21 to 7 ka, while accommodation due to tectonic deformation appears to have become more important as the rate of sea-level rise slowed after ~7 ka. On the bathymetrically flat inner shelf, where energetic ocean conditions rework and transport sediments offshore, variation in sediment thickness is primarily due to tectonically induced relief. On the mid to outer shelf, where aggradation is observed, the rate of sediment supply plays a larger role in generating alongshore variations in sediment thickness. Although stratal geometry and bathymetry show little evidence of a transition to the highstand systems tract in the near-shore (<20 m), the building up of relief offshore the Eel River in water depths ~40 m indicates the transition from the transgressive systems tract to the highstand systems tract has occurred. The geometry of reflectors within the transgressive sequence indicates the relative timing of sediment accumulation and deformation; offset of the transgressive surface and diverging reflectors in the upper transgressive sediments indicate that deposition is syntectonic with rates of up to approximately 3 mm/yr in the Eel River Syncline. Onshore to offshore correlation of deformation structures is tenuous as many structures onshore appear to die away offshore and those offshore appear to die off onshore, attesting to the complex three-dimensional deformation in the region. Although it has been recognized that coastlines can exhibit alternating transgressive and highstand regimes alongshore, this work demonstrates that tectonic deformation and oceanographic conditions can create similar variability from onshore to offshore. Clearly the integration of seismics, cores, and bathymetry is necessary to unravel the controls on sediment dispersal in tectonically complex settings.

Acknowledgements

This project was funded by ONR as part of the STRATAFORM initiative and an Achievement Rewards for College Scientists (ARCS) fellowship. The authors would like to thank Alan Orpin for thoughtful reviews and an anonymous reviewer for their contribution. Special thanks to Joe Kravitz and the Los Angeles ARCS Foundation.

References

Alexander, C.R., Simoneau, A.M., 1999. Spatial variability in sedimentary processes on the Eel continental slope. Marine Geology 154, 243–254.
Atwater, T., 1970. Implications of plate tectonics for the Cenozoic tectonic evolution of western North America. Geological Society of America Bulletin 81, 3513–3536.
Atwater, T., Stock, J., 1998. Pacific-North America plate tectonics of the Neogene, southwestern United States; an update. International Geology Review 40, 375–402.
Baldwin, W.E., Morton, R.A., Denny, J.F., Dadisman, S.V., Schwab, W.C., Gayes, P.T., Driscoll, N.W., 2004. Maps showing the stratigraphic framework of South Carolina's Long Bay from Little River to Winyah Bay: U.S. Geological Survey Open-File Report 04–1013.
Bard, E., Hamelin, B., Fairbanks, R.G., Zindler, A., 1990. Calibration of the 14-C timescale over the past 30,000 years using mass spectrometric U-Th ages from Barbados corals. Nature 345, 405–409.
Bard, E., et al., 1996. Deglacial sea-level record from Tahiti corals and the timing of global meltwater discharge. Nature 382 (6588), 241–244.
Brothers, D.S., Driscoll, N.W., Kent, G.M., Harding, A.J., Babcock, J.M., Baskin, R.L., 2009. Tectonic evolution of the Salton Sea inferred from seismic reflection data. Nature Geoscience 2, 581–584.
Brown, W.M., Ritter, J., 1971. Sediment Transport and Turbidity in the Eel River Basin. California. U.S, Geological Survey Water Supply Paper. 1986.
Burger, R.L., Fulthorpe, C.S., Austin, J.A., Gulick, S.P.S., 2002. Lower Pleistocene to present structural deformation and sequence stratigraphy of the continental shelf, offshore Eel River Basin, northern California. Marine Geology 185 (3–4), 249–281.
Catuneanu, O., 2006. Principles of Sequence Stratigraphy. Elsevier, Amsterdam. 375 pp.
Christie-Blick, N., Driscoll, N.W., 1995. Sequence stratigraphy. Annual Review of Earth and Planetary Sciences 23, 451–478.
Clarke, S.H., 1992. Geology of the Eel River Basin and adjacent region—implications for Late Cenozoic Tectonics of the Southern Cascadia Subduction Zone and Mendocino Triple Junction. American Association of Petroleum Geologists Bulletin 76 (2), 199–224.
Clarke, S.H., Carver, G.A., 1992. Late Holocene Tectonics and Paleoseismicity, Southern Cascadia Subduction Zone. Science 255 (5041), 188–192.
Cohen, J.K., Stockwell Jr., J.W., 1999. CWP/SU: Seismic Unix Release 33: a free package for seismic research and processing, software. Center for Wave Phenomena, Colorado School of Mines, Golden, CO.
Driscoll, N.W., Hogg, J.R., 1995. Stratigraphic response to basin formation: Jeanne d'Arc Basin, offshore Newfoundland. Geological Society, London, Special Publications: v. 80, 145–163.
Driscoll, N.W., Karner, G.D., 1999. Two-dimensional quantitative modeling of Clinoform development. Marine Geology 154, 383–398.
Fan, S., Swift, D.J.P., Traykovski, P., Bentley, S., Borgeld, J.C., Reed, C.W., Niedoroda, A.W., 2004. River flooding, storm resuspension, and event stratigraphy on the northern California shelf: observations compared with simulations. Marine Geology 210, 17–41.
Fairbanks, R.G., 1990. The age and origin of the "Younger Dryas climate event" in Greenland ice cores. Paleoceanography 5 (6), 937–948.
Fairbanks, R., 1992. Barbados Sea Level and Th/U 14C Calibration. IGBP PAGES/World Data Center for Paleoclimatology Data Contribution Series # 92-020. NOAA/NGDC Paleoclimatology Program, Boulder CO, USA.
Ferrini, V., Flood, R.D., 2002. Multibeam Sonar on the Inner Shelf of the Eel Margin: nearshore gravel-floored troughs. Eos, Transactions, American Geophysical Union 83 (47) Fall Meeting Supplement, Abstract OS71C-0297.
Gerber, T.P., Lincoln, P.F., Kuehl, S., Walsh, J.P., Alexander, C., Palmer, A., 2010. The influence of sea level and tectonics on Late Pleistocene through Holocene sediment storage along the high-sediment supply Waipaoa continental shelf. Marine Geology 270, 139–159.
Goff, J.A., Orange, D.L., Mayer, L.A., Clarke, J.E.H., 1999. Detailed investigation of continental shelf morphology using a high-resolution swath sonar survey: the Eel margin, northern California. Marine Geology 154 (1–4), 255–269.
Grossman, E.E., Eittreim, S.L., Field, M.E., Wong, F.L., 2006. Shallow stratigraphy and sedimentation history during high-frequency sea-level changes on the central California shelf. Continental Shelf Research 26, 1217–1239.
Gulick, S.P.S., Meltzer, A.S., 2002. Effect of the northward-migrating Mendocino triple junction on the Eel River forearc basin, California: structural evolution. Geological Society of America Bulletin 114 (12), 1505–1519.
Harris, C.K., Traykovski, P.A., Geyer, W.R., 2005. Flood dispersal and deposition by near-bed gravitational sediment flows and oceanographic transport: a numerical modeling study of the Eel River shelf, northern California. Journal of Geophysical Research-Oceans 110, C09025.
Havholm, K.G., Ames, D.V., Whittecar, G.R., Wenell, B.A., Riggs, S.R., Jol, H.M., Berger, G.W., Holmes, M.A., 2004. Stratigraphy of back-barrier coastal dunes, northern North Carolina and southern Virginia. Journal of Coastal Research 20 (4), 980–999.
Henkart, P., 2003. SIOSEIS, software. Scripps Institution of Oceanography. La Jolla, CA. available at http://sioseis.ucsd.edu.
Hogarth, L.J., Babcock, J., Driscoll, N.W., Le Dantec, N., Hass, J.K., Inman, D.L., Masters, P.M., 2007. Long-term tectonic control on Holocene shelf sedimentation offshore La Jolla, California. Geology 35 (3), 275–278.
Jin, J.H., Chough, S.K., 1998. Partitioning of transgressive deposits in the southeastern Yellow Sea: a sequence stratigraphic interpretation. Marine Geology 149 (1–4), 79–92.
Karner, G.D., Driscoll, N.W., Weissel, J.K., 1993. Response of the lithosphere to in-plane force variations. Earth and Planetary Science Letters 114, 397–416.
Kelsey, H.M., Carver, G.A., 1988. Late Neogene and Quaternary tectonics associated with northward growth of the San-Andreas transform-fault, Northern California. Journal of Geophysical Research-Solid Earth and Planets 93 (B5), 4797–4819.

Labaune, C., Tesson, M., Gensous, B., 2008. Variability of the transgressive stacking pattern under environmental changes control: example from the Post-Glacial deposits of the Gulf of Lions inner-shelf, Mediterranean, France. Continental Shelf Research 28 (9), 1138–1152.

Le Dantec, N., Hogarth, L.J., Driscoll, N.W., Babcock, J.M., Barnhardt, W.A., Schwab, W.C., 2010. Tectonic controls on nearshore sediment accumulation and submarine canyon morphology offshore La Jolla, southern California. Marine Geology 268, 115–128.

Lea, D.W., Martin, P.A., Pak, D.K., Spero, H.J., 2002. Reconstructing a 350 ky history of sea level using planktonic Mg/Ca and oxygen isotopic records from a Cocos Ridge core. Quaternary Science Reviews 21 (1–3), 283–293.

Lobo, F.J., Hernandez-Molina, F.J., Somoza, L., Diaz del Rio, V., 2001. The sedimentary record of the post-glacial transgression on the Gulf of Cadiz continental shelf (Southwest Spain). Marine Geology 178 (1–4), 171–195.

McCrory, P.A., 2000. Upper plate contraction north of the migrating Mendocino triple junction, northern California: Implications for partitioning of strain. Tectonics 19 (6), 1144–1160.

McLaughlin, R.J., Ellen, S.D., Blake Jr., M.C., Jayko, A.S., Irwin, W.P., Aalto, K.R., Carver, G.A., Clarke Jr., S.H., 2000. Geology of the Cape Mendocino, Eureka, Garberville, and Southwestern Part of the Hayfork 30 × 60 Minute Quadrangles and Adjacent Offshore Area, Northern California. USGS Miscellaneous Field Studies MF–2336, Version 1.0.

Nittrouer, C.A., 1999. STRATAFORM: overview of its design and synthesis of its results. Marine Geology 154 (1–4), 3–12.

Orange, D.L., 1999. Tectonics, sedimentation, and erosion in northern California: submarine geomorphology and sediment preservation potential as a result of three competing processes. Marine Geology 154 (1–4), 369–382.

O'Shea, D., 2005. Continental shelf sedimentation and Holocene development of the northern California coast, Eel River and Humboldt Bay: Masters Thesis, Humboldt State University.

Posamentier, H.W., Allen, G.P., 1993. Variability of the sequence stratigraphic model: effects of local basin factors. Sedimentary Geology 86, 91–109.

Posamentier, H.W., Allen, G.P., 1994. Siliciclastic sequence stratigraphic patterns in foreland ramp-type basins. Geology 21, 455–458.

Posamentier, H.W., Jervey, M.T., Vail, P.R., 1988. Eustatic controls on clastic deposition I—conceptual frameworks. In: Wilgus, C.K., Hastings, B.S., Kendall, C.G.S.C., Posamentier, H.W., Foss, C.A., Van Wagoner, J.C. (Eds.), Sea-level changes: an integrated approach society of economic paleontologists and mineralogists special publication no. 42, pp. 39–45.

Posamentier, H.W., Vail, P.R., 1988. Eustatic controls on clastic deposition II—sequence and systems tract models. In: Wilgus, C.K., Hastings, B.S., Kendall, C.G.S.C., Posamentier, H.W., Foss, C.A., Van Wagoner, J.C. (Eds.), Sea-level changes: an integrated approach society of economic paleontologists and mineralogists special publication no. 42, pp. 39–45.

Sloss, L.L., 1963. Sequences in the cratonic interior or North America. Geological Society of America Bulletin 74, 93–114.

Sommerfield, C.K., Nittrouer, C.A., 1999. Modern accumulation rates and a sediment budget for the Eel shelf: a flood-dominated depositional environment. Marine Geology 154 (1–4), 227–241.

Sommerfield, C.K., Wheatcroft, R.A., 2007. Late Holocene sediment accumulation on the northern California shelf: Oceanic, fluvial, and anthropogenic influences. Geological Society of America Bulletin 119 (9–10), 1120–1134.

Spinelli, G.A., Field, M.E., 2003. Controls of tectonics and sediment source locations on along-strike variations in transgressive deposits on the northern California margin. Marine Geology 197 (1–4), 35–47.

Swift, D.J.P., Phillips, S., Thorne, J.A., 1991. Sedimentation on continental margins. Part V: Parasequences. In: Swift, D.J.P., Tillman, R.W., Oertel, G.F., Thorne, J.A. (Eds.), Shelf sand and sandstone bodies: geometry, facies and sequence stratigraphy: International Association of Sedimentologists Special Publication, 14, pp. 153–187.

Syvitski, J.P., Morehead, M.D., 1999. Estimating river-sediment discharge to the ocean: application to the Eel margin, northern California. Marine Geology 154, 13–41.

Trincardi, F., Correggiari, A., Roveri, M., 1994. Late Quaternary transgressive erosion and deposition in a modern epicontinental shelf: the Adriatic Semienclosed Basin. Geo-Marine Letters 14, 41–51.

Unruh, J., Humphrey, J., Barron, A., 2003. Transtensional model for the Sierra Nevada frontal fault system, eastern California. Geology 31 (4), 327–330.

Vail, P.R., Mitchum, R.M., Thompson, S., 1977. Seismic stratigraphy and global changes of sea level, part 3: Relative changes of sea level from coastal onlap. In: Payton, C.E. (Ed.), Seismic stratigraphy—applications to hydrocarbon exploration: Tulsa, Oklahoma, American Association of Petroleum Geologists Memoir, 26, pp. 63–81.

Van Wagoner, J.C., Mitchum, R.M., Campion, K.M., Rahmanian, V.D., 1990. Siliciclastic sequence stratigraphy in well logs, cores, and outcrops: Tulsa, Oklahoma. American Association of Petroleum Geologists Methods in Exploration Series. No. 7, 55 pp.

Vick, G.S. 1988. Late Holocene paleoseismicity and relative sea level changes of the Mad River Slough, Northern Humboldt Bay, California: Masters Thesis, Humboldt State University.

Wheatcroft, R.A., Sommerfield, C.K., 2005. River sediment flux and shelf sediment accumulation rates on the Pacific Northwest margin. Continental Shelf Research 25 (3), 311–332.

Wheatcroft, R.A., Sommerfield, C.K., Drake, D.E., Borgeld, J.C., Nittrouer, C.A., 1997. Rapid and widespread dispersal of flood sediment on the northern California margin. Geology 25 (2), 163–166.

Yun, J.W., Orange, D.L., Field, M.E., 1999. Gas distribution in the Eel River Basin and its link to submarine geomorphology. Marine Geology 154, 357–368.

Zhang, Y., Swift, D.J.P., Fan, S.J., Niedoroda, A.W., Reed, C.W., 1999. Two-dimensional numerical modeling of storm deposition on the northern California shelf. Marine Geology 154 (1–4), 155–167.